The Catalytic Copper of Peptidylglycine α-Hydroxylating Monooxygenase also Plays a Critical Structural Role

Xavier Siebert,* Betty A. Eipper,† Richard E. Mains,† Sean T. Prigge,‡ Ninian J. Blackburn,§ and L. Mario Amzel*
*Biophysics and Biophysical Chemistry, Johns Hopkins University School of Medicine, Baltimore, Maryland; †Neuroscience, University of Connecticut Health Center, Farmington, Connecticut; ‡Molecular Microbiology and Immunology, Johns Hopkins University School of Public Health, Baltimore, Maryland; and §Environmental and Biomolecular Systems, OGI School of Science and Engineering, Oregon Health and Science University, Beaverton, Oregon

ABSTRACT Many bioactive peptides require amidation of their carboxy terminus to exhibit full biological activity. Peptidylglycine α-hydroxylating monooxygenase (PHM; EC 1.14.17.3), the enzyme that catalyzes the first of the two steps of this reaction, is composed of two domains, each of which binds one copper atom (CuH and CuM). The CuM site includes Met^{314} and two His residues as ligands. Mutation of Met^{314} to Ile inactivates PHM, but has only a minimal effect on the EXAFS spectrum of the oxidized enzyme, implying that it contributes only marginally to stabilization of the CuM site. To characterize the role of Met^{314} as a CuM ligand, we determined the structure of the Met^{314}Ile-PHM mutant. Since the mutant protein failed to crystallize in the conditions of the original wild-type protein, this structure determination required finding a new crystal form. The Met^{314}Ile-PHM mutant structure confirms that the mutation does not abolish CuM binding to the enzyme, but causes other structural perturbations that affect the overall stability of the enzyme and the integrity of the CuH site. To eliminate possible effects of crystal contacts, we redetermined the structure of wt-PHM in the Met^{314}Ile-PHM crystal form and showed that it does not differ from the structure of wild-type (wt)-PHM in the original crystals. Met^{314}Ile-PHM was also shown to be less stable than wt-PHM by differential scanning calorimetry. Both structural and calorimetric studies point to a structural role for the CuM site, in addition to its established catalytic role.

INTRODUCTION

Many bioactive peptides require a carboxy-terminal α-amide ($CONH_2$) for activity (for reviews, see (1–3)). Peptide amidation is catalyzed by a single, bifunctional enzyme named PAM (EC 1.14.17.3), short for peptidylglycine α-amidating monooxygenase. PAM is composed of two enzymatic domains: peptidylglycine α-hydroxylating monooxygenase (PHM; EC 1.14.17.3) and peptidyl-α-hydroxyglycine amidating lyase (PAL; EC 4.3.2), that act sequentially on a glycine-extended propeptide as shown in Fig. 1 (4).

The reaction catalyzed by PHM has been extensively studied using a variety of techniques, including x-ray crystallography (5,6), extended x-ray absorption fine spectroscopy (EXAFS) (7,8), electron paramagnetic resonance (7,9), fluorescence (10), kinetic analysis (11), and mutagenesis (7). PHM is a dicopper monooxygenase that catalyzes the stereospecific α-hydroxylation of the peptidylglycine substrate by molecular oxygen (O_2). The two copper atoms, CuH (also named CuA) and CuM (also named CuB), are essential for activity (12) and cycle between Cu(I) and Cu(II) during catalysis (9). Reduction of the copper ions is carried out independently by two molecules of ascorbate, which are oxidized to semidehydroascorbate. Each copper contributes one electron to the overall reaction, and the required electron transfer between the copper sites only occurs in the presence of both substrate and dioxygen (9).

X-ray diffraction studies of PHMcc, the catalytic core of the PHM domain of rat PAM-1 (residues 42–356, hereafter referred to as PHM for simplicity) (13), have shown that the two copper atoms are 11 Å apart, separated by a solvent-filled cleft (5). CuH coordination is unusual and can be described as square pyramidal with three histidines (His^{107}, His^{108}, His^{172}) and two unoccupied positions (''T-shape'' coordination). By contrast, CuM is coordinated by two histidines (His^{242}, H^{244}), a methionine (Met^{314}) and a water molecule (or OH^-) in a slightly distorted tetrahedral geometry. Comparison of the reduced and oxidized structures shows only minor changes (C_α root mean-square deviation (RMSD) $\approx$ 0.2 Å), even in the coordination of the copper ions (slight motion of His^{108} only).

However, recent EXAFS experimental data (14) were interpreted as indicating a significant lengthening of the $Met^{314}S_\gamma$ to CuM distance from 2.25 Å in the reduced form to 2.8 Å in the oxidized form. In the crystallographic structures (5,6,15), the corresponding distances are either 2.27Å (Protein Data Bank (PDB)-1sdw) or 2.45 Å (PDB-3phm) in the reduced form and either 2.38Å (PDB-1opm) or 2.42Å (PDB-1phm) in the oxidized form.

Mutation of Met^{314} to Ile (Met^{314}Ile) inactivates PHM (7), but this substitution results in minimal changes in the EXAFS spectrum of the oxidized enzyme (14), implying that methionine coordination contributes minimally to the stabilization of Cu(II) at the CuM site. Upon reduction, EXAFS and absorption edge data show significant differences between Met^{314}Ile-PHM and wild-type (wt)-PHM (14). Previous studies also showed that substitution of Met^{314} with His or

Submitted May 11, 2005, and accepted for publication July 19, 2005.

Address reprint requests to L. Mario Amzel, E-mail: mario@neruda.med.jhmi.edu.

0006-3495/05/11/3312/08 $2.00

doi: 10.1529/biophysj.105.066100

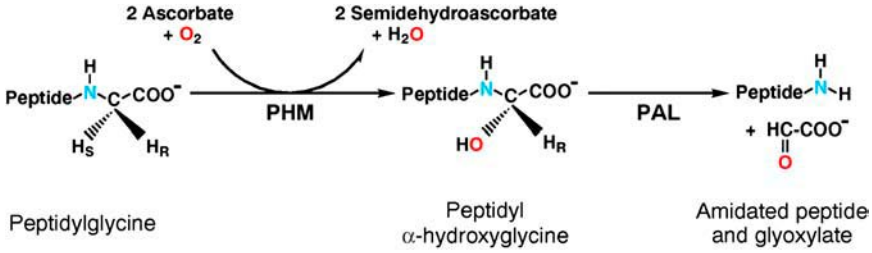

FIGURE 1 Overall mechanism of PAM, showing the sequential action of its two catalytic domains, PHM and PAL, on a glycine-extended propeptide.

Cys (that could potentially still bind CuM) did not restore catalytic activity (13).

To explore further the role of the Met^{314} ligand, we determined the structures of the $Met^{314}Ile$ mutant in both oxidized (ox-$Met^{314}Ile$-PHM) and reduced (red-$Met^{314}Ile$-PHM) states. Since the $Met^{314}Ile$-PHM protein does not crystallize under the same conditions as wt-PHM (PDB-1opm, 1phm, 3phm, 1sdw), we redetermined the oxidized and reduced structures of wt-PHM in the new crystal form (ox-wt-PHM and red-wt-PHM, respectively), to eliminate the possibility of artifacts due to crystal contacts.

To evaluate the effect of the $Met^{314}Ile$ mutation on the stability of the enzyme, we measured the excess heat capacity ($C_{p,ex}$) of wt-PHM and of $Met^{314}Ile$-PHM as a function of temperature using differential scanning calorimetry (DSC). Both structural and calorimetric studies point to a structural role for the CuM site, in addition to its established catalytic role.

MATERIAL AND METHODS

Protein expression and purification

Stably transfected Chinese hamster ovary (CHO) cell lines secreting PHMcc were constructed using the pCIS vector system as described before (13). Details of cell culture and protein purification, copper reconstitution and activity measurements were provided elsewhere (5,7). Stably transfected cell lines carrying the $Met^{314}Ile$ mutation were constructed as reported previously (7). The $Met^{314}Ile$-PHM purification and copper reconstitution were described before (14,16).

Protein crystallization and diffraction data collection

Purified $Met^{314}Ile$-PHM and wt-PHM were concentrated to 15 mg/ml in 50 mM Na-Hepes (pH 6.8) and 50 mM NaCl. Since $Met^{314}Ile$-PHM did not crystallize in the conditions published for wt-PHM (5) (525 μM $CuSO_4$, 3.08 mM NaN_3, 100 mM dimethylarsinic acid pH 5.5, at 298 K), we found new crystallization conditions with incomplete factorial screening using hanging-drop vapor-diffusion at 293K. $Met^{314}Ile$ crystals appeared after a week in drops composed of 2 μl of protein and 2 μl of a reservoir solution containing 27% (w/v) PEG-4000, 600 mM $MgCl_2$, 100 mM Tris pH 8.5. Crystals were frozen at 93 K in the reservoir solution with added 5 mM $CuSO_4$ and 30% glycerol as cryoprotectant. Diffraction data were collected on single frozen crystals, either at a home source (Rigaku RU-200 rotating anode generator and R-AXIS IV image plate detector) or at a beam line (X25 or X26C) of the National Synchrotron Light Source at Brookhaven National Laboratory (Upton, NY) (Table 1). Data reduction was carried out using the programs MOSFLM and SCALA from the CCP4 suite (17).

The $Met^{314}Ile$ crystals belong to the orthorhombic space group $P2_12_12_1$ with unit cell dimensions $a = 59.5$ Å, $b = 66.5$ Å, $c = 70.0$ Å, $\alpha = \beta = \gamma = 90°$ and one $Met^{314}Ile$-PHM molecule per asymmetric unit. The $Met^{314}Ile$ crystal form differs from that of the original wt-PHM crystals (5) ($a = 69.4$ Å, $b = 68.8$ Å, $c = 81.0$ Å, $\alpha = \beta = \gamma = 90°$, space group $P2_12_12_1$). To compare $Met^{314}Ile$-PHM and wt-PHM in the same crystal form, crystals of wt-PHM were grown in the new crystallization conditions using microseeding techniques. These crystals also belong to the orthorhombic space group $P2_12_12_1$ with unit cell dimensions highly similar to those of the $Met^{314}Ile$ crystals ($a = 58.5$ Å, $b = 65.7$ Å, $c = 69.9$ Å, $\alpha = \beta = \gamma = 90°$). Data collection statistics are given in Table 1.

Structure refinement

The same overall procedure was used for all four structures (ox-$Met^{314}Ile$-PHM, red-$Met^{314}Ile$-PHM, ox-wt-PHM, red-wt-PHM): the published coordinates of wt-PHM (PDB-1opm for the oxidized state and PDB-3phm for the reduced state) were positioned in the unit cell with the program AMoRe (18) and used as the starting model for alternate cycles of model building and refinement using the programs O (19) and REFMAC5.0 (20). Five percent of the reflections were set aside from the beginning of the refinement to calculate the R_{free} values. Solvent molecules were added automatically using ARP/WARP (21) and visually inspected with the program O (19). The geometrical integrity of the structures was checked throughout refinement using the program MolProbity (22). The crystallographic statistics are summarized in Table 1.

Differential scanning calorimetry

Measurements for wild-type PHM and the $Met^{314}Ile$-PHM mutant were carried out on a VP-DSC microcalorimeter (MicroCal, Northampton, MA) at the Biocalorimetry Center of the Johns Hopkins University (Baltimore, MD). The scanning rate was 60°/h. Proteins (wt and $Met^{314}Ile$) were concentrated to 0.1 mg/ml in buffers containing 50 mM MES pH 6.8, 50 mM NaCl, and 5 μM $CuSO_4$. Protein and buffer solutions were properly degassed and carefully loaded into the cells to avoid bubble formation.

RESULTS AND DISCUSSION

Overall structure of ox-$Met^{314}Ile$-PHM

Structural alignment (C_α RMSD = 0.947 Å) between ox-$Met^{314}Ile$-PHM and the published structure of oxidized wt-PHM (PDB-1opm) shows differences in the N-terminus and in the 177–182 region (Fig. 2), but the most relevant main-chain changes are located close to the CuM site: the mutated residue Ile^{314} is displaced away from CuM, causing the flanking loop (299-313) to become highly disordered (*dashed lines* in Fig. 2) and the loop 212-218 to move away from CuM (C_α of Gly^{217} displaced by as much as 5 Å). The

TABLE 1 Statistics of crystallographic analysis and refinement

	Ox-wt-PHM	Red-wt-PHM	Ox-Met^{314}Ile-PHM	Red-Met^{314}Ile-PHM
Data collection				
Wavelength (Å)	1.54	1.10	1.10	1.10
X-ray source	Home	X25	X25	X26C
Space group	$P2_12_12_1$	$P2_12_12_1$	$P2_12_12_1$	$P2_12_12_1$
No. of observed reflections	65470	85900	61959	49563
No. of unique reflections	14082	19172	28704	11215
Redundancy	4.7 (4.7)	4.5 (4.7)	2.5 (1.4)	4.5 (4.6)
Completeness (%)	92.9 (90.4)	99.5 (99.9)	87.6 (48.8)	99.5 (99.7)
Signal $\langle(I/\sigma(I))\rangle$	18.8 (2.18)	9.2 (3.0)	8.8 (1.8)	4.3 (1.7)
R_{sym} (%)	5.8 (44.4)	5.4(23.9)	4.1 (37.5)	6.5 (44.5)
Resolution (Å)	2.2	2.0	1.7	2.4
Model composition (nonhydrogen atoms)				
No. of amino acids	45–355	47–355	47–355	50–355
No. of active site Cu	2	2	2	0
No. of water molecules	154	83	130	47
No. of total atoms	2581	2505	2469	2319
Refinement				
R_{cryst} (%)	18.6	19.0	19.6	18.8
R_{free} (%)	25.0	26.1	23.3	27.1
Stereochemistry				
Root mean-square for bond length (Å)	0.042	0.024	0.026	0.033
Root mean-square for bond angles (deg)	3.0	2.2	2.3	2.7
$\langle B\rangle$(Å^2)	33.1	33.4	41.7	51.3

Numbers in parenthesis correspond to the last resolution shell. X-ray sources are either a home source (Rigaku RU-200 rotating anode generators and R-AXIS IV image plate detectors) or a beam line (X25 or X26C) of the National Synchrotron Light Source, Brookhaven National Laboratory (red, reduced; ox, oxidized).

$$R_{sym} = \sum_{hkl}\sum_i |I(hkl) - \langle I(hkl)\rangle|/\sum_{hkl}\sum_i |I(hkl)|.$$

$$R_{cryst} = \sum_{hkl} ||F_{obs}(hkl)| - F_{calc}(hkl)||/\sum_{hkl}|F_{obs}(hkl)|.$$

R_{free} was calculated as in Brünger (32), using 5% of the data for the test set.

effect of the mutation on the stability of the 299-313 loop does not propagate to residues past Met^{314}, because Cis^{315} is constrained by a disulfide bridge to Cis^{293} (see Fig. 3).

It may be argued that these changes are the result of crystal packing differences between PDB-1opm and ox-Met^{314}Ile-PHM because different crystal forms were used to determine these structures. In PDB-1opm, wt-PHM crystallizes with an adventitious crystal contact involving His^{305} from one molecule, His^{235} from a symmetry-related molecule, and three components from the crystallization buffer: a Ni^{2+} ion, an azide molecule and a glycerol molecule (Fig. 2, *inset*). Importantly, His^{305} is located in the middle of the 299-313 loop that is disordered in ox-Met^{314}Ile-PHM, which does not require Ni^{2+} for crystallization, has different unit cell dimensions and uses different crystal contacts.

To find out unambiguously whether the destabilization of the loop is caused by the loss of the crystal contact involving His^{305} or by the Met^{314}Ile mutation itself, we redetermined the oxidized and reduced structures of wt-PHM in the Met^{314}Ile-PHM crystal form (see Methods and Table 1). We refer to the new oxidized and reduced structures as ox-wt-PHM and red-wt-PHM, respectively.

Redetermination of the structure of oxidized wt-PHM

The oxidized structures of wt-PHM in the two crystal forms (ox-wt-PHM and PDB-1opm, Fig. 4) have a C_α RMSD of 0.721 Å, the difference being mostly located in the regions that were shifted in the ox-Met^{314}Ile-PHM structure (Fig. 2). The shifts in N-terminus and in the loop 174-184 are similar in ox-wt-PHM and ox-Met^{314}Ile-PHM (Figs. 2 and 4) and can thus be attributed to the change in crystal form. The change in the loops 212-218 and 305-313 is less pronounced in ox-wt-PHM than in ox-Met^{314}Ile-PHM, and therefore results mostly from the mutation.

Most importantly, the 299-313 loop of ox-wt-PHM is well ordered ($\langle B\rangle$= 34.4 Å^2 for ox-wt-PHM and 38.3 Å^2 for the PDB-1opm), showing that the cause of the destabilization of the 299-313 loop in ox-Met^{314}Ile-PHM is the mutation Met^{314}Ile flanking the loop, and not the change in crystal contacts. It is interesting to note that the structure of wt-PHM at pH 8.5 (ox-wt-PHM) is very similar to that at the physiological pH 5.5 (PDB-1opm), with essentially identical copper binding sites. This finding validates the results of ex-

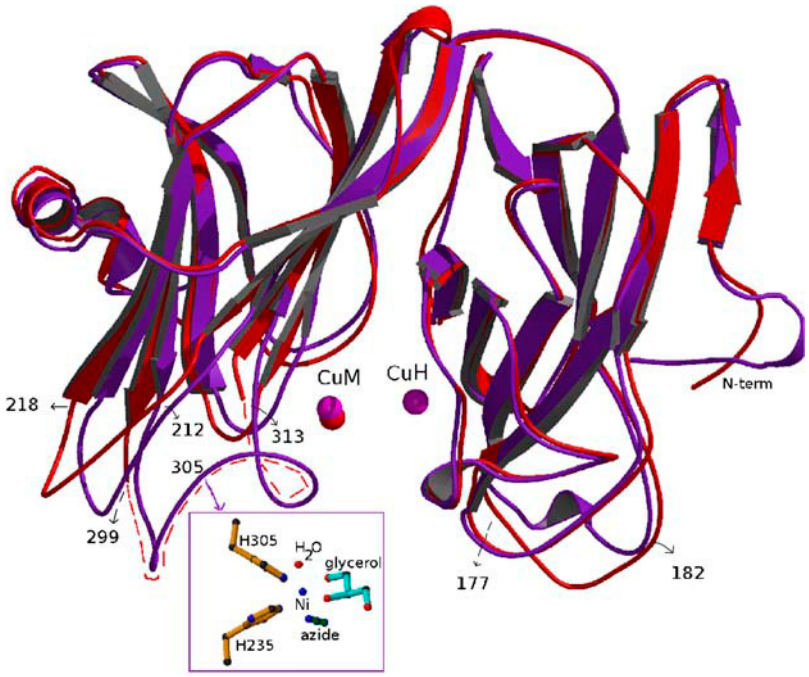

FIGURE 2 Superposition of the structures of PDB-1opm (*magenta*) and ox-Met^{314}Ile-PHM (*red*). Labeled residues delimit regions where the main chains PDB-1opm and ox-Met^{314}Ile-PHM differ significantly. The dashed region represents the loop 299-313 that is too disordered to be traced in Met^{314}Ile-PHM. The insert depicts the adventitious crystal contact in PDB-1opm that involves His^{305}, a Ni^{2+} ion, an azide molecule, a glycerol molecule (from the crystallization buffer), and His^{235} (from a symmetry-related molecule). Ribbon diagrams were generated with MolScript (33).

periments performed at a nonphysiological pH (e.g., EXAFS performed at pH 7.5 (7,8)).

Effects of the Met^{314}Ile mutation on the active site

Surprisingly, removal of the Met^{314} ligand to CuM does not abolish the binding of CuM, as shown by the spherical anomalous diffraction difference Fourier density found at the position of CuM in ox-Met^{314}Ile-PHM (Fig. 5 *A*). The CuM site in ox-Met^{314}Ile-PHM (Fig. 5 *A*) accommodates the mutation by replacing Met^{314}S$_\gamma$ with a water molecule, and by shifting the positions of the other coordinating residues (His^{242}, His^{244}, and a water molecule), to form a distorted tetrahedron. Some disorder can be observed at the CuM site as a result of the mutation: the B-factors are higher than average for CuM and for the N$_\epsilon$ of His^{242} and His^{244} (65 Å^2, 55 Å^2, and 60 Å^2; $\langle$B (protein)$\rangle$ = 37.8 Å^2) and at lower contour levels, the anomalous diffraction difference Fourier map around CuM becomes elongated in the direction perpendicular to the line joining the N$_\epsilon$ of His^{242} and His^{244} (data not shown).

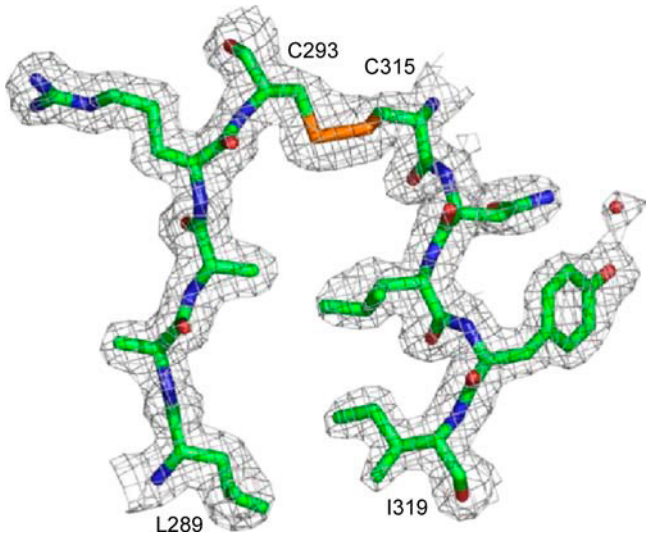

FIGURE 3 Region next to the Met^{314}Ile mutation (residues 315–319) and the neighboring chain (residues 293–289) in the ox-Met^{314}Ile structure, showing the disulfide bridge between C315 and C293 and the electron density map, contoured at 1 σ. This figure was prepared with PyMOL (34).

Unexpectedly, the CuH site appears to be much more affected by the Met^{314}Ile mutation than the CuM site, even though the two copper ions are 11 Å apart, without any significant structural change in the protein regions connecting them (Fig. 4). In particular, His^{107} and CuH are highly disordered in the ox-Met^{314}Ile-PHM structure, and refined to occupancies of 30% with B-factors 39 Å^2 and 54 Å^2, respectively. The anomalous signal of CuH is weaker than that of CuM; the anomalous diffraction difference Fourier map around CuH differs significantly from a spherical shape (Fig. 5 *A*), indicating disorder and/or partial occupancy. Only two histidines (His^{108} and His^{172}) coordinate CuH linearly, whereas His^{107} is disordered, as confirmed by the Fo-Fc omit map (contoured at 2 σ; Fig. 5 *B*) generated from a model that omitted both copper atoms and their coordinating residues.

Fig. 5, *C* and *D*, show that both copper sites of the ox-wt-PHM structure (same crystal form as ox-Met^{314}Ile-PHM) are essentially identical to those of PDB-1opm, proving that the changes observed in the ox-Met^{314}Ile-PHM structure at CuH and CuM are caused by the Met^{314}Ile mutation, and not by the change in crystal contacts. The electron density map in

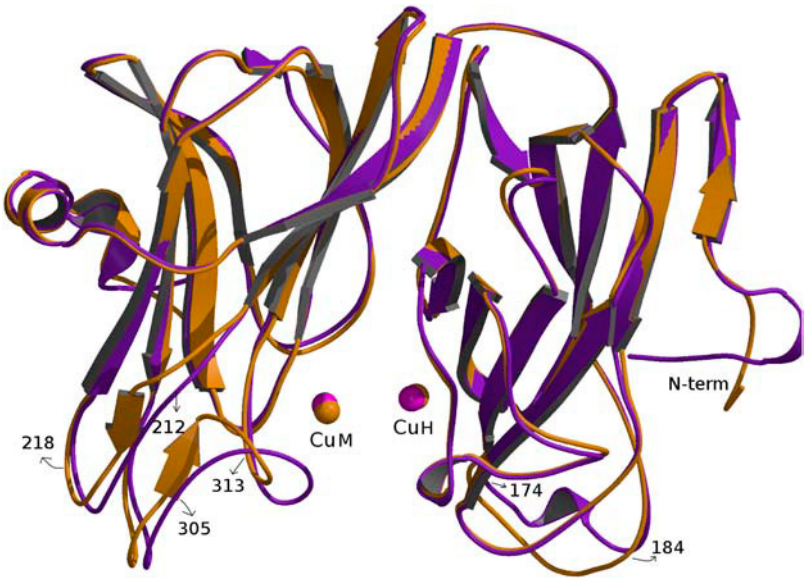

FIGURE 4 Superposition of the structures of PDB-1opm (*magenta*) and ox-wt-PHM (*mustard*). Labeled residues delimit regions where the main chains PDB-1opm and ox-wt-PHM differ significantly. Ribbon diagrams were generated with MolScript (33).

Fig. 3 showing a well ordered region of the Met^{314}Ile-PHM structure can serve as evidence of the overall quality of the data, giving credence to the structural changes shown in Fig. 5, *A* and *B*. During this study, several data sets were collected, both at a home source and at the synchrotron, and all of them systematically revealed that the mutation at CuM propagates to CuH (data not shown).

EXAFS studies (14) have also detected mobility of a His ligand to CuH, resulting in a linear coordination of this copper in the reduced form of the protein. Although the mobile histidine was assumed to be His^{172} (8,14), the disorder observed in the crystal structure for His^{107} assigns this role to His^{107}. Other published reports have also suggested a connection between the properties of the two copper sites. For example, coupling of the movement of Met^{314} to the occupancy of the CuH site has been observed by EXAFS (23), and carbon monoxide (CO) binding studies (16) have shown that binding of substrate near CuM favors binding of CO to CuH. Together, these data highlight a structural role of the CuM site that has far-reaching implications on the integrity of the CuH site.

Differential scanning calorimetry

To evaluate the effect of the Met^{314}Ile mutation on the overall stability of the PHM protein, we investigated the thermal denaturation of wt-PHM and of Met^{314}Ile-PHM using differential scanning calorimetry. Both proteins denatured irreversibly (Fig. 6), probably due to the loss of Cu upon unfolding, but their behavior is significantly different. The denaturation is centered at a lower temperature for the mutant than for the native (75.9°C for wt-PHM and 73°C for Met^{314}Ile-PHM), indicating that the loss of the CuM-S bond has an important destabilizing effect on the structure of PHM.

Structural role of CuM site

The structural and calorimetric data indicate that the Met^{314}Ile mutation perturbs the stability of the enzyme, which in turn affects the ability of copper to bind to the CuH site. This suggests that the CuH site in wt-PHM is tailored to hold copper in its unusual coordination, and is therefore sensitive to the overall stability of the protein. By contrast, CuM forms a stable complex with only the two histidines, as observed in the structure of Met^{314}Ile-PHM. This partial complex is able to bind to the S atom of Met^{314} and use this bond to anchor the loop containing residues 299–314 against the copper, adding stability to the protein and preforming the CuH binding site. Interestingly, the Glu^{313}Asp mutant shows altered catalytic properties (data not shown), possibly because it also destabilizes the 299-313 loop. The mechanistic importance of the stabilizing Met^{314}-CuM interaction has also been predicted by density functional calculations (24,25).

Thus, the CuM site plays a significant structural role, in addition to its established catalytic function (15). Copper ions usually play catalytic roles in enzymes, although they have been shown to be important structurally in some cases such as the type 3 active site copper of human ceruloplasmin (26) and hemocyanin (27). PHM therefore offers a rare example of a copper site playing major structural and catalytic roles.

Structural effects of reduction

The structure of red-Met^{314}Ile-PHM shows that upon reduction the mutant loses both CuH and CuM, as indicated by the lack of anomalous signal (see Supplementary Material). In addition, all active-site histidines become more mobile. These effects appear to be caused by the mutation and not by the crystal contacts, since red-wt-PHM retains both copper

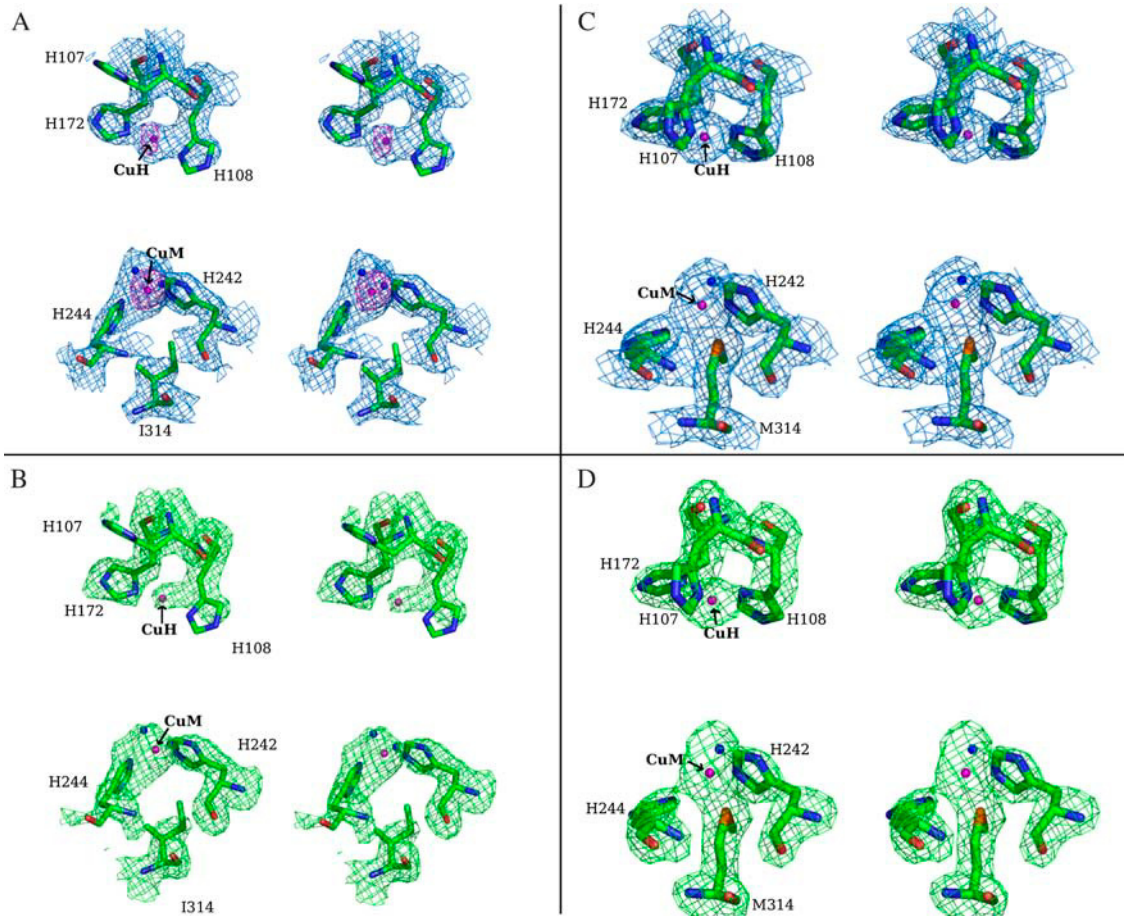

FIGURE 5 Comparison (using cross-eyed stereo views) of the active sites of ox-Met^{314}Ile-PHM (*A* and *B*) and ox-wt-PHM (*C* and *D*). Copper atoms and water molecules are represented as pink and blue spheres, respectively. (*A*) Ox-Met^{314}Ile-PHM with the 2 Fo-Fc electron density map (*blue*), contoured at 0.9 σ and the anomalous diffraction difference Fourier map (*pink*), contoured at 4 σ. (*B*) Ox-Met^{314}Ile-PHM with Fo-Fc difference Fourier map (*green*), contoured at 1.8 σ and generated from a model that omitted all the atoms in *A*. (*C*) Ox-wt-PHM with the 2 Fo-Fc electron density map (*blue*), contoured at 1 σ. (*D*) Ox-wt-PHM with Fo-Fc difference Fourier map (*green*) contoured at 2.5 σ and generated from a model that omitted all the atoms in *C*. This figure was prepared with PyMOL (34).

ions upon reduction (see Supplementary Material). The reduced structures of red-wt-PHM and PDB-3phm differ only in the conformations of the loops 174-184, 212-218, and 299-313 (C_α RMSD = 0.940 Å) and no main-chain conformational changes are observed in the protein region connecting the two copper sites. As in ox-Met^{314}Ile-PHM, the 299-313 loop flanking the mutation is highly disordered in red-Met^{314}Ile-PHM. This observation is further evidence that reduction does not trigger major conformational changes during the catalytic cycle: in two crystal forms, with different crystal contacts, no major structural differences are observed between the oxidized and the reduced forms.

SUMMARY AND CONCLUSIONS

The crystal structure of Met^{314}Ile-PHM reveals that in addition to its established catalytic role, the CuM site of PHM plays an essential role in the structural integrity of the enzyme. This effect is confirmed by the lower thermal stability of the mutant enzyme with respect to the wild-type, as measured by DSC. The structural role of CuM in PHM appears to be twofold. First, CuM anchors the active conformation of the 299-314 loop and, as shown by the DSC experiment, the CuM-Met^{314} coordination stabilizes the protein. Second, the stabilized structure has a preformed CuH site that allows copper to bind with an unusual coordination. This arrangement may be important for adjusting the electrochemical potentials of reduced CuH and CuM to favor electron transfer, as shown in the constrained coordination of blue copper proteins (28). The effect of the coordination of the CuM site on the ordering of the CuH site is remarkable, because CuH and CuM are located 11 Å apart, on opposite faces of a solvent-filled cleft. Neither the Met^{314}Ile mutation nor reduction causes major conformational change in the region of the protein connecting the two copper sites. These results also clarify previous results of EXAFS experiments that detected motion of a histidine ligand to CuH upon reduction of Met^{314}Ile-PHM (14).

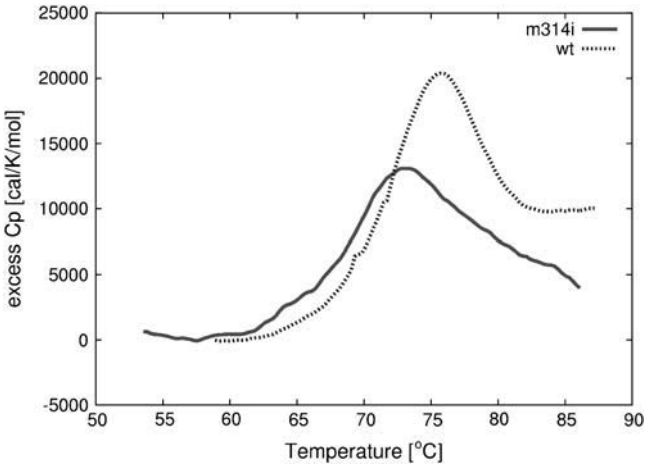

FIGURE 6 Excess heat capacity as a function of temperature for the wt-PHM and Met^{314}Ile-PHM proteins, after substraction of the baseline corresponding to the buffer scan.

During this study, a new crystal form of the wt-PHM was obtained. Despite differences in crystal contacts, the structures of wt-PHM (in the oxidized and the reduced state) in the new crystal form are essentially identical to those of the equivalent structures in the previously reported crystal form. These observations add further support to previous studies arguing against mechanisms involving major conformational changes during the catalytic cycle of PHM. Since PHM shares 32% sequence identity with dopamine-β-monooxygenase (29) and has similar cofactor requirements (30) and kinetics (11), mechanistic insights obtained with each enzyme have been used interchangeably (31). Findings of the studies on PHM presented here are expected to apply to dopamine-β-monooxygenase as well.

SUPPLEMENTARY MATERIAL

An online supplement to this article can be found by visiting BJ Online at http://www.biophysj.org.

We thank Dr. M. Becker and the staff at beam lines X25 and X26C for assistance during data collection at the National Synchrotron Light Source, Brookhaven National Laboratory, which is supported by the U.S. Department of Energy, Division of Materials Sciences and Division of Chemical Sciences, under contract No. DE-AC02-98CH10886. We thank Dr. Arne Schön for performing the DSC experiments and Dr. Ernesto Freire for the use of the equipment at the Biocalorimetry Center. This work was supported by National Science Foundation grant No. MCB-9982945 (L.M.A. and S.T.P.) and National Institutes of Health grant No. DK32949 (B.A.E. and R.E.M.).

Coordinates have been submitted to the Protein Data Bank (accession numbers: 1YIP = ox-wt-PHM, 1YI9 = ox-M^{314}I-PHM, 1YJK = red-wt-PHM, 1YJL = red-M^{314}I-PHM).

REFERENCES

1. Cuttitta, F. 1993. Peptide amidation: signature of bioactivity. *Anat. Rec.* 236:87–93.
2. Eipper, B. A., D. A. Stoffers, and R. E. Mains. 1992. The biosynthesis of neuropeptides: peptide α-amidation. *Annu. Rev. Neurosci.* 15:57–85.
3. Merkler, D. J. 1994. C-terminal amidated peptides: production by the in vitro enzymatic amidation of glycine-extended peptides and the importance of the amide to bioactivity. *Enzyme Microb. Technol.* 16: 450–456.
4. Bradbury, A. F., M. D. Finnie, and D. G. Smyth. 1982. Mechanism of C-terminal amide formation by pituitary enzymes. *Nature.* 298:686–688.
5. Prigge, S. T., A. S. Kolhekar, B. A. Eipper, R. E. Mains, and L. M. Amzel. 1997. Amidation of bioactive peptides: the structure of peptidylglycine alpha-hydroxylating monooxygenase. *Science.* 278: 1300–1305.
6. Prigge, S. T., A. S. Kolhekar, B. A. Eipper, R. E. Mains, and L. M. Amzel. 1999. Substrate-mediated electron transfer in peptidylglycine alpha-hydroxylating monooxygenase. *Nat. Struct. Biol.* 6:976–983.
7. Eipper, B. A., A. S. Quon, R. E. Mains, J. S. Boswell, and N. J. Blackburn. 1995. The catalytic core of peptidylglycine alpha-hydroxylating monooxygenase: investigation by site-directed mutagenesis, Cu x-ray absorption spectroscopy, and electron paramagnetic resonance. *Biochemistry.* 34:2857–2865.
8. Jaron, S., R. E. Mains, B. A. Eipper, and N. J. Blackburn. 2002. The catalytic role of the copper ligand H172 of peptidylglycine alpha-hydroxylating monooxygenase (PHM): a spectroscopic study of the H172A mutant. *Biochemistry.* 41:13274–13282.
9. Freeman, J. C., J. J. Villafranca, and D. J. Merkler. 1993. Redox cycling of enzyme-bound copper during peptide amidation. *J. Am. Chem. Soc.* 115:4923–4924.
10. Bell, J., R. El Meskini, D. D'Amato, R. E. Mains, and B. A. Eipper. 2003. Mechanistic investigation of peptidylglycine alpha-hydroxylating Monooxygenase vias intrinsic tryptophan fluorescence and mutagenesis. *Biochemistry.* 42:7133–7142.
11. Francisco, W. A., D. J. Merkler, N. J. Blackburn, and J. P. Klinman. 1998. Kinetic mechanism and intrinsic isotope effects for the peptidylglycine alpha-amidating enzyme reaction. *Biochemistry.* 37:8244–8252.
12. Kulathila, R., A. P. Consalvo, P. F. Fitzpatrick, J. C. Freeman, L. M. Snyder, J. J. Villafranca, and D. J. Merkler. 1994. Bifunctional peptidylglcine alpha-amidating enzyme requires two copper atoms for maximum activity. *Arch. Biochem. Biophys.* 311:191–195.
13. Kolhekar, A. S., H. T. Keutmann, R. E. Mains, A. S. Quon, and B. A. Eipper. 1997. Peptidylglycine alpha-hydroxylating monooxygenase: active site residues, disulfide linkages, and a two-domain model of the catalytic core. *Biochemistry.* 36:10901–10909.
14. Blackburn, N. J., F. C. Rhames, M. Ralle, and S. Jaron. 2000. Major changes in copper coordination accompany reduction of peptidylglycine monooxygenase: implications for electron transfer and the catalytic mechanism. *J. Biol. Inorg. Chem.* 5:341–353.
15. Prigge, S. T., B. A. Eipper, R. E. Mains, and L. M. Amzel. 2004. Dioxygen binds end-on to mononuclear copper in a precatalytic enzyme complex. *Science.* 304:864–867.
16. Jaron, S., and N. J. Blackburn. 1999. Does superoxide channel between the copper centers in peptidylglycine monooxygenase? A new mechanism based on carbon monoxide reactivity. *Biochemistry.* 38:15086–15096.
17. The ccp4 suite: programs for protein crystallography. Collaborative computational project number 4. 1994. *Acta Cryst.* D50:760–763.
18. Navaza, J. 1994. AMoRe: an automated package for molecular replacement. *Acta Crystallogr.* A50:157–163.
19. Jones, T. A., Z.-Y. Zou, S. W. Cowan, and M. Kjeldgaard. 1991. Improved methods for the building of protein models in electron density maps and the location of errors in these models. *Acta Crystallogr.* A47:110–119.
20. Murshudov, G. N., A. A. Vagin, and E. J. Dodson. 1997. Refinement of macromolecular structures by the maximum-likelihood method. *Acta Crystallogr.* D53:240–255.

21. Lamzin, V. S., and K. S. Wilson. 1997. Automated refinement for protein crystallography. *Methods Enzymol.* 277:269–305.

22. Lovell, S. C., I. W. Davis, W. B. Arendall III, P. I. W. de Bakker, J. M. Word, M. G. Prisant, J. S. Richardson, and D. C. Richardson. 2003. Structure validation by c-alpha geometry: phi, psi, and c-beta deviation. *Proteins Struct. Funct. Genet.* 50:437–450.

23. Jaron, S., and N. J. Blackburn. 2001. Characterization of a half-apo derivative of peptidylglycine monooxygenase. Insight into the reactivity of each active site copper. *Biochemistry.* 40:6867–6875.

24. Chen, P., J. Bell, B. A. Eipper, and E. I. Solomon. 2004. Oxygen activation by the noncoupled binuclear copper site in peptidylglycine alpha-hydroxylating monooxygenase. Spectroscopic definition of the resting sites and the putative CuIIM-OOH intermediate. *Biochemistry.* 43:5735–5747.

25. Chen, P., and E. I. Solomon. 2004. Oxygen activation by the noncoupled binuclear copper site in peptidylglycine alpha-hydroxylating monooxygenase. Reaction mechanism and role of the noncoupled nature of the active site. *J. Am. Chem. Soc.* 126:4991–5000.

26. Vachette, P., E. Dainese, V. B. Vasyliev, P. Di Muro, M. Beltramini, D. I. Svergun, V. De Filippis, and B. Salvato. 2002. A key structural role for active site type 3 copper ions in human ceruloplasmin. *J. Biol. Chem.* 277:40823–40831.

27. Gatto, S., V. De Filippis, F. Spinozzi, P. Di Muro, L. Bubacco, and M. Beltramini. 2004. Structural role of the copper ions in the dinuclear active site of Carcinus aestuarii hemocyanin. *Micron.* 35:43–44.

28. Gray, H. B., B. G. Malmstrom, and R. J. Williams. 2000. Copper coordination in blue proteins. *J. Biol. Inorg. Chem.* 5:551–559.

29. Southan, C., and L. I. Kruse. 1989. Sequence similarity between dopamine beta-hydroxylase and peptide alpha-amidating enzyme: evidence for a conserved catalytic domain. *FEBS Lett.* 255:116–120.

30. Eipper, B. A., R. E. Mains, and C. C. Glembotski. 1983. Identification in pituitary tissue of a peptide alpha-amidation activity that acts on glycine-extended peptides and requires molecular oxygen, copper, and ascorbic acid. *Proc. Natl. Acad. Sci. USA.* 80:5144–5148.

31. Prigge, S. T., R. E. Mains, B. A. Eipper, and L. M. Amzel. 2000. New insights into copper monooxygenases and peptide amidation: structure, mechanism and function. *Cell. Mol. Life Sci.* 57:1236–1259.

32. Brünger, A. T. 1992. Free R value: a novel statistical quantity for assessing the accuracy of crystal structures. *Nature.* 355:472–475.

33. Kraulis, P. J. 1991. MolScript: a program to produce both detailed and schematic plots of protein structures. *J. Appl. Crystallogr.* 24:946–950.

34. DeLano, W. L. 2002. The PyMOL Molecular Graphics System. http://www.pymol.org, W.L. DeLano Scientific, San Carlos, CA.